

Translational Characterization of [^{11}C]GSK931145, a PET Ligand for the Glycine Transporter Type 1

ROGER N. GUNN,^{1,2,3*} VENKATESHA MURTHY,⁴ ANA M. CATAFAU,⁴ GRAHAM SEARLE,¹ SANTIAGO BULLICH,⁵ MARK SLIFSTEIN,⁶ DANIELE OUELLET,⁷ STEFANO ZAMUNER,⁷ RAUL HERANCE,⁵ CRISTIAN SALINAS,¹ RICARDO PARDO-LOZANO,⁸ EUGENII A. RABINER,^{1,2} MAGI FARRE,⁸ AND MARC LARUELLE^{2,4,6}

¹GlaxoSmithKline, Clinical Imaging Center, Hammersmith Hospital, London, United Kingdom

²Division of Neuroscience and Mental Health, Imperial College, London, United Kingdom

³Department of Engineering Science, University of Oxford, United Kingdom

⁴GlaxoSmithKline, Neurosciences Center of Excellence for Drug Discovery, Harlow, United Kingdom; Barcelona, Spain

⁵CRC-CIM & Institut d'Alta Tecnologia-PRBB, Barcelona, Spain

⁶Department of Psychiatry, Columbia University, New York

⁷GlaxoSmithKline, Clinical Pharmacology Modelling and Simulation, Stockley Park, United Kingdom; RTP, North Carolina

⁸Clinical Pharmacology Unit, IMIM-Hospital del Mar, Autonomous University of Barcelona, Barcelona, Spain

KEY WORDS drug occupancy; GlyT-1; [^{11}C]GSK931145; positron emission tomography; test–retest

ABSTRACT The current interest in developing Glycine transporter Type 1 (GlyT-1) inhibitors, for diseases such as schizophrenia, has led to the demand for a GlyT-1 PET molecular imaging tool to aid drug development and dose selection. We report on [^{11}C]GSK931145 as a novel GlyT-1 imaging probe in primate and man. Primate PET studies were performed to determine the level of specific binding following homologous competition with GSK931145 and the plasma-occupancy relationship of the GlyT-1 inhibitor GSK1018921. Human PET studies were performed to determine the test–retest reproducibility of [^{11}C]GSK931145 and the plasma-occupancy relationship of GSK1018921. [^{11}C]GSK931145 entered primate and human brain and yielded a heterogeneous pattern of uptake which was similar in both species with highest uptake in midbrain, thalamus, and cerebellum. Homologous competition in primates indicated no viable reference region and gave binding potential estimates between 1.5 and 3 for midbrain, thalamus and cerebellum. While the distribution and binding potential values were similar across species, both the plasma free fraction (f_P : 0.8 vs. 8%) and delivery (K_1 : 0.025 vs. 0.126 ml cm⁻³ min⁻¹) were significantly lower in humans. Test–retest reproducibility in humans calculated using a two tissue compartmental model was poor (VAR(V_T): 29–38%), but was improved using a pseudo reference tissue model (VAR(BP_{ND}): 16–23%). GSK1018921 EC₅₀ estimates were 22.5 and 45.7 ng/ml in primates and humans, respectively. **Synapse 65:1319–1332, 2011.** © 2011 Wiley-Liss, Inc.

INTRODUCTION

The *N*-methyl *D*-aspartate (NMDA) receptor is an ionotropic glutamate receptor that includes recognition sites for glycine and glutamate. Glutamate acts as the primary neurotransmitter and glycine is an obligatory coagonist. Glycine enhances the affinity and efficacy of glutamate, as well as delaying receptor desensitization and increasing the frequency and duration of NMDA receptor channel opening. Synaptic levels of glycine are regulated by two high affinity glycine transporter subtypes, referred to as GlyT-1

and GlyT-2, which share ~50% amino acid sequence identity.

GlyT-1 is expressed throughout the body, although its expression in the central nervous system (CNS) is

Contract grant sponsor: GlaxoSmithKline

*Correspondence to: Roger N. Gunn, GlaxoSmithKline, Clinical Imaging Center, Imperial College London, Hammersmith Hospital, Du Cane Road, London W12 0NN, United Kingdom. E-mail: roger.n.gunn@gsk.com

Received 11 May 2011; Revision 7 June 2011; Accepted 10 June 2011

DOI 10.1002/syn.20966

Published online 17 June 2011 in Wiley Online Library (wileyonlinelibrary.com).

relatively widespread and much greater than in the periphery. In contrast, the distribution of GlyT-2 is relatively limited, being present mainly on inhibitory glycinergic neurons in the spinal cord, brainstem and cerebellum. GlyT-1 is present on both glial and neuronal cells (Aragon et al., 2005; Cubelos et al., 2005) in the CNS where it provides the principal high affinity transport system controlling extracellular glycine levels. At least three isoforms of GlyT-1 exist (GlyT-1a, GlyT-1b, and GlyT-1c), which differ at their extreme N-termini and may vary in their distribution, expression or developmental regulation; however, there is no evidence that these isoforms differ in their functional properties or pharmacology.

GlyT-1 inhibition has been shown, both in vitro and in vivo, to promote downstream processes related to NMDA receptor function such as synaptic plasticity (e.g., long-term potentiation), a cellular process that provides a significant contribution to the physiological processes underlying learning and memory. In the clinic, sarcosine (*N*-methyl glycine), a natural amino acid that acts as a low potency GlyT-1 inhibitor has been reported to produce improvements in all three symptom domains of schizophrenia (positive, negative, and cognitive) when used as adjunctive therapy in patients stabilized on typical or atypical antipsychotics (Tsai et al., 2004). More potent GlyT-1 inhibitors are currently being developed for the symptomatic treatment of schizophrenia.

The current interest in developing GlyT-1 inhibitors has led to the demand for a GlyT-1 positron emission tomography (PET) molecular imaging tool to aid pre-clinical/clinical development and dose selection. Recently, [^{11}C]GSK931145 was identified as a promising radioligand for imaging GlyT-1 in the pig, as it possessed good brain penetration, specific signal and reversible kinetics (Passchier et al., 2010) and has been shown to have suitable dosimetry for human studies (Bullich et al., 2010). Hamill et al. (2010) have also recently presented [^{18}F]MK-6577 as a promising GlyT-1 tracer in rhesus monkey. Here, we report on the translation of [^{11}C]GSK931145 into primate and man including characterization of specific and nonspecific binding, development of quantitative analysis methods, assessment of test–retest reproducibility, and its application to drug development studies designed to assess occupancy of novel GlyT-1 assets.

MATERIALS AND METHODS

Primate studies were performed at Columbia University to determine (i) the level of specific binding following homologous competition with high doses (0.5 mg/kg) of GSK931145 and (ii) the plasma-occupancy relationship of the novel GlyT-1 inhibitor GSK1018921 at a range of doses (0.03–0.5 mg/kg). Human studies were performed at the Barcelona Imag-

ing Unit in collaboration with CRC-CIM and IMIM to determine (iii) the test–retest reproducibility of [^{11}C]GSK931145 and (iv) the plasma-occupancy relationship of GSK1018921 at a range of doses (25–200 mg).

Radiochemistry

[^{11}C]GSK931145 was radiolabeled by methylation and prepared at both sites according to methods described previously (Bullich et al., 2010).

Primate studies

All data were acquired under protocols approved by the Columbia University Medical Center Institutional Animal Care and Use Committee (IACUC). In total, four subjects (*Papio Anubis*) (23.2 ± 3.3 kg) were scanned as part of these experiments. Eight pairs of scans were performed in total. Each scan pair involved a baseline and postdrug scan; $2 \times$ GSK931145 (0.5 mg/kg) and $6 \times$ GSK1018921 (2×0.03 , 1×0.125 , and 3×0.5 mg/kg). Fasted animals were immobilized with ketamine (10 mg/kg i.m.) and anesthetized with 2% isoflurane via endotracheal tube. A venous cannula was inserted for hydration and tracer delivery. An arterial cannula was inserted in the femoral artery for blood sampling. Vital signs were monitored and body temperature was maintained at 37°C with heated water blankets.

PET data were acquired on a Siemens HR+ scanner (Siemens, Knoxville, TN; Resolution: FWHM = 4.3 mm at the center of the field of view, Brix et al., 1997). All sessions consisted of a 120 min scan, followed by a 60-min infusion of the challenge compound, followed by a 120-min postchallenge scan. A 10-min transmission scan using a ^{68}Ge rod source was acquired prior to each session for attenuation correction. Dynamic data were acquired in 3D mode (4×15 s, 2×1 min, 3×2 min, 2×5 min, and 10×10 min). Data were reconstructed by filtered backprojection using a Shepp filter (0.5 cycles/ray) following corrections for decay, attenuation (using the transmission scan data), subtraction of randoms, and modeled scatter correction (Watson, 1996).

Arterial plasma was sampled with an automated fraction collection system for the first 4 min (12 samples, 1 every 20 s) followed by manual draws at longer intervals for the remainder of the scan. Six additional samples at 2, 4, 12, 20, 40, and 70 min were collected for metabolite analysis by high-performance liquid chromatography (HPLC) using a fraction collection method. Additional plasma samples were taken to measure the concentration of GSK1018921 and these were analyzed with an HPLC/MS/MS assay.

Parent fractions were fitted to the Hill equation $f = 1 - at^b/(c + t^b)$ where t is time and a , b , and c are fitted parameters. The total plasma concentration of radioactivity was corrected with this function, and

the resultant curve was fitted (from the time of peak activity) to a sum of three exponential functions and used as the plasma input function for kinetic analysis.

PET data were coregistered to T1-weighted magnetic resonance imaging (MRI) images acquired for each baboon (three-dimensional gradient recall, TR = 34 ms, TE = 4 ms, flip angle = 45°, slice thickness = 1 mm, pixel dimensions = 0.5 × 0.5 mm²) on a 1.5 T GE Signa Excite Twinspeed scanner (GE Healthcare, Little Chalfont, Buckinghamshire, UK). Regions of interest (ROIs) were manually drawn on the MRI images using MEDx software (Medical Numerics, Germantown, MD) and included cortex (temporal), cerebellum, midbrain, and thalamus. Coregistration was performed by maximization of mutual information, as implemented in the SPM2 software package (Wellcome Trust Center for Neuroimaging, <http://www.fil.ion.ucl.ac.uk/spm>). ROIs were applied to coregistered dynamic PET data and time activity curves (TACs) derived. Kinetic analysis was then applied (see below).

Human studies

Thirteen human healthy volunteers (age 24 ± 3 years, range 20–30 years, [6 male, 7 female]) out of 17 who enrolled completed the test–retest study, and 10 separate male volunteers (age 28 ± 6 years, range 23–42 years) out of 11 enrolled completed the GSK1018921 occupancy study. All subjects in the test–retest study underwent two separate baseline [¹¹C]GSK931145 PET scans at least 1 week apart (interval: 11.37 ± 4.38 days), and all subjects in the GSK1018921 occupancy study underwent three [¹¹C]GSK931145 PET scans—one at baseline and two at different time points following a single oral dose of GSK1018921 (doses ranged between 25 and 200 mg, times post dose ranged between 2 and 48 h and were selected using an adaptive optimal design (Zamuner et al., 2010). The timing of scans postdose were adapted twice during the study and the first time point ranged between 2 and 12 h and the second time point ranged between 10 and 48 h). None of the subjects enrolled had past or present psychiatric disorders as assessed by the Structured Clinical Interview for DSM (IV)-TR (SCID-(IV)) questionnaire (First et al., 2002). None were taking psychotropic drugs or other relevant medication. All had normal findings on physical examination, 12-lead electrocardiography, clinical chemistry, hematology, and urine analysis. Absence of illegal drug abuse was assessed by history and supported by urine drug screening and alcohol breath test on the day of the PET scans. The study was approved by the local Research Ethics Committee (CEIC-IMAS) and the Spanish Ministry of Health (Spanish Medicines Agency, AEMPS). All subjects

provided written informed consent before inclusion in the study.

PET was performed using a Siemens ECAT-EXACT HR+ camera equipped with transmission sources of ⁶⁸Ge. Prior to [¹¹C]GSK931145 injection, a 10-min transmission scan was obtained for attenuation correction. After injection of [¹¹C]GSK931145, 120 min of dynamic emission data were acquired (frames: 8 × 15 s, 3 × 60 s, 5 × 120 s, 5 × 300 s, and 8 × 600 s). The PET data were corrected for decay, attenuation, scatter, randoms, dead time and reconstructed using filtered back projection with a Hanning filter (kernel FWHM of 4.9 mm).

A structural T1-weighted MRI scan was acquired for all subjects (axial three-dimensional spoiled gradient echo: repetition time, 25 ms; echo time, 6 ms; flip angle, 28°).

Arterial blood activity was measured every second for the first 15 min after injection using a continuous sampling system (ABSS Allogg, Mariefred, Sweden). Thereafter, 15 manual samples were collected at the following time points: 5, 10, 14, 17, 22.5, 27.5, 32.5, 37.5, 45, 55, 65, 75, 85, 95, and 110 min to assay whole blood and plasma activity (plasma was obtained following centrifugation over 10 min at 1800 g) in a gamma counter (Perkin Elmer Wallac, Waltham, MA; Wizard 1470 Automatic Gamma Counter). Three samples collected at 5, 10, and 14 min after injection, which overlapped the continuous blood sampling period, were used to calibrate continuous blood samples to match discrete samples and the data were combined into a single whole-blood activity curve. The sampled plasma data were divided by the corresponding whole-blood measurements and the average of these values was taken as the plasma-over-blood ratio. The whole blood curve was multiplied by this value to obtain a total plasma activity curve.

The parent fraction of [¹¹C]GSK931145 was measured by HPLC for eight plasma samples (5, 10, 17.5, 27.5, 45, 65.5, 95, and 110 min) and was fitted to a single exponential plus a constant. The total plasma activity was multiplied by this parent fraction and then smoothed postpeak by fitting to a tri-exponential function to generate an arterial parent plasma input. Additional plasma samples were taken at the start and end of each post drug PET scan to measure the concentration of GSK1018921 and these were analyzed with an HPLC/MS/MS assay.

Dynamic PET data were corrected for motion via frame-to-frame image registration, using frame 20 (30–35 min) as the reference frame, and aligned with the structural T1 MRI image using SPM5 (Wellcome Trust Center for Neuroimaging, <http://www.fil.ion.ucl.ac.uk/spm>) with a mutual information cost function. The CIC neuroanatomical atlas (Tziortzi et al., 2010) was nonlinearly deformed into the individual's space to obtain a personalized anatomical parcellation of

ROIs and subsequently, via application to the dynamic emission data, TACs for a comprehensive set of regions. Attention focused on regions of moderate and high binding: midbrain, thalamus, and cerebellum, and on a global cortex region of interest (ROI) representing low binding regions.

Kinetic analysis

Both primate and human data sets were analyzed by a one and two tissue compartment model (1TC, 2TC) with arterial plasma input using programs developed in-house with Matlab software. A fixed 5% blood volume contribution was subtracted from data prior to analysis. The primary outcome measures were the radioligand delivery (K_1 ; mL cm⁻³ min⁻¹) and the total distribution volume (V_T ; mL cm⁻³). Due to the ubiquitous distribution of GlyT-1, no reference region was available and so the occupancy plot (Cunningham et al., 2010; Lassen et al., 1995) was used to determine estimates of drug occupancy.

Additional analyses were performed with a newly developed pseudo reference tissue model (PRTM) approach which does not require the reference region to be devoid of specific binding. While previous work has examined the effect of specific binding in a reference region on the outcome measures derived from the target regions of interest (Asselin et al., 2007; Christian et al., 2004; Olsson et al., 2004), methods have not been explicitly developed to correct for this effect. We introduce PRTM approaches (Eqs. 1 and 2 below) which enable the corrected estimate of BP_{ND} or occupancy and apply these to the human data sets. The PRTM takes a region with the lowest target expression as the reference and makes a correction for the level of binding in this region. This assumes that the V_{ND} in the target and pseudo reference regions are equal and that the binding potential at baseline (BP_{ND}^R) in the pseudo reference region can be estimated from additional competition data. Assessment of a wide range of regions derived from application of the CIC neuroanatomical template (Tziortzi et al., 2010) to the PET data was used to identify the pseudo reference region as the region with lowest mean V_T value across the study population.

When no true reference region exists, the total volume of distribution in the reference region (R) can be expressed as $V_T^R = V_{ND} + V_S^R$, and in the target tissue (T) as $V_T^T = V_{ND} + V_S^T$. The binding potentials in the target and reference regions can be expressed as BP_{ND}^T = V_S^T/V_{ND} and BP_{ND}^R = V_S^R/V_{ND} respectively. Let BP_{ND}^M denote the binding potential measured for T by treating R as a true reference region (BP_{ND}^M = $(V_T^T - V_T^R)/V_T^R$), then:

$$BP_{ND}^T = BP_{ND}^R + BP_{ND}^M(1 + BP_{ND}^R). \quad (1)$$

For baseline (or test-retest) data, this correction can be applied directly using an estimate of baseline BP_{ND}^R. A corresponding correction for occupancy can be derived as:

$$Occ = Occ^M \cdot \left(\frac{1 + BP_{ND}^R}{1 + BP_{ND}^R \cdot Occ^M} \right), \quad (2)$$

where BP_{ND}^R is the baseline binding potential in the pseudo reference region and Occ^M is the occupancy calculated by treating R as a true reference region (Occ^M = $1 - BP_{ND}^{M2}/BP_{ND}^{M1}$, where BP_{ND}^{M1} and BP_{ND}^{M2} are the binding potentials measured for the target tissue from baseline and postdose scans, respectively). Full derivations of Eqs. 1 and 2 are given in the appendix.

The relationship between the plasma concentration of GSK1018921 at the start of the scan ($C_P^{GSK1018921}$) and occupancy was fitted by an E_{max} model, for both the primate and human data sets, using the method of least squares,

$$Occ = \frac{C_P^{GSK1018921}}{EC_{50} + C_P^{GSK1018921}} \quad (3)$$

Reproducibility of the human test-retest data were quantified by variability (VAR: the mean of $([2ABS(test - retest)]/[test + retest])$) and intraclass correlation coefficient (ICC; Kirk, 1982).

RESULTS

[¹¹C]GSK931145 was successfully synthesized at high specific activity for both primate (injected activity: 105 ± 44 MBq (range 46–195), injected mass: 0.88 ± 0.16 µg) and human studies (injected activity: 429 ± 158 MBq (range 146–673), injected mass: 4.78 ± 2.34 µg. Ten out of 13 subjects provided two evaluable PET data sets in the test-retest study, and analysis results from 10 subjects are presented for each of the test-retest and occupancy studies.

Primate studies

Following i.v. injection in the primate there was rapid distribution throughout the brain with GlyT-1 rich areas such as brain stem, thalamus, and cerebellum, demonstrating increased uptake when compared with cortical regions (Figs. 1A and 1D). The tracer was metabolized throughout the scanning period and intact parent radioligand comprised ~30% (average over all scans) of the radioactive signal in arterial plasma after 1 h (Figs. 1B and 1C). The 2TC model was chosen as an appropriate model based on Akaike model selection criteria (for brevity, only 2TC results are reported). The 2TC model was successfully fitted

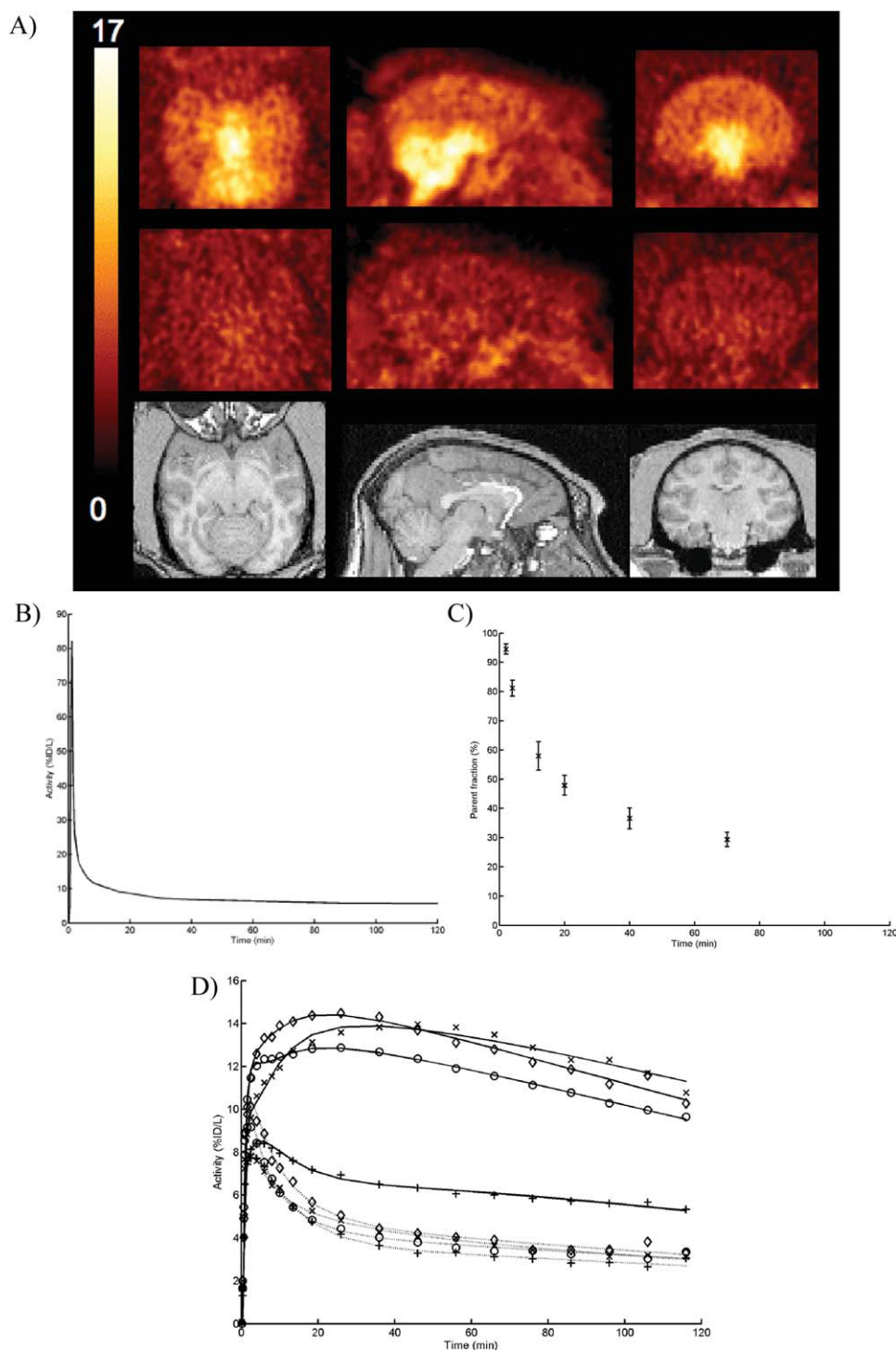


Fig. 1. [^{11}C]GSK931145 Primate data: Homologous competition data (A,D). (A) Heterogeneous distribution in brain with high uptake in brain stem, thalamus, and cerebellum at baseline (top row) homogeneous distribution following blocking with 0.5 mg/kg cold GSK931145 (middle row) and structural MRI (bottom). Units are %ID/L. (B) Metabolite corrected arterial plasma time course for

[^{11}C]GSK931145. (C) Measured [^{11}C]GSK931145 fraction in plasma samples. (D) Regional TACs (thalamus (\diamond), cerebellum (\circ), mid brain (\times), and cortex ($+$)) and two tissue compartment model fits from baseline scan (solid lines) and following blockade with 0.5 mg/kg GSK931145 (dotted lines).

to TACs derived from cortical, cerebellar, thalamic, and midbrain regions to derive parameter estimates (Fig. 1D; Table I). The V_T estimates were well identi-

fied for all four regions across all subjects as indicated by the asymptotic error estimates (mean $\% \text{COV}(V_T) = 2.34\%$). Estimates of tracer delivery were similar

TABLE I. Quantitative analysis of [^{11}C]GSK931145 primate studies involving homologous block with GSK931145 and competition with GSK1018921

Dose	Pk conc (ng/ml)	Midbrain (V_T)	Thalamus (V_T)	Cerebellum (V_T)	Cortex (V_T)	Occupancy plot analysis		
						Occupancy	V_{ND}	R^2
Baseline		7.25	6.57	6.02	3.33			
0.5 mg/kg	GSK931145	1.72	1.86	1.73	1.57	94.6%	1.49	0.999
Baseline		5.8	5.51	5.12	2.95			
0.5 mg/kg	GSK931145	1.72	1.54	1.66	1.3	86.9%	1.06	0.998
Baseline		4.1	3.72	4.01	2.1			
0.03 mg/kg	GSK1018921	5.44	3.78	3.48	1.94	8.2%	0.92	0.260
Baseline		4.16	3.87	3.73	2.36			
0.5 mg/kg	GSK1018921	9.33	2.15	1.74	1.21	50.7%	0.04	0.979
Baseline		4.23	3.52	3.5	1.96			
0.125 mg/kg	GSK1018921	10.5	3.03	2.66	1.85	47.7%	1.74	0.999
Baseline		4.62	5.09	4.25	2.03			
0.03 mg/kg	GSK1018921	14	5.14	4.28	2.29	20.0%	3.82	0.468
Baseline		4.98	4.55	4.22	2.22			
0.5 mg/kg	GSK1018921	94.7	2.32	2.01	1.62	76.6%	1.41	0.998
Baseline		3.85	3.56	3.85	2.16			
0.5 mg/kg	GSK1018921	220.7	1.68	1.64	1.28	77.9%	1.02	0.999
Baseline (mean)		4.87	4.55	4.34	2.39			
Baseline (SD)		1.14	1.10	0.83	0.49			

V_T estimates were derived from a 2TC analysis and occupancy estimates from the occupancy plot.

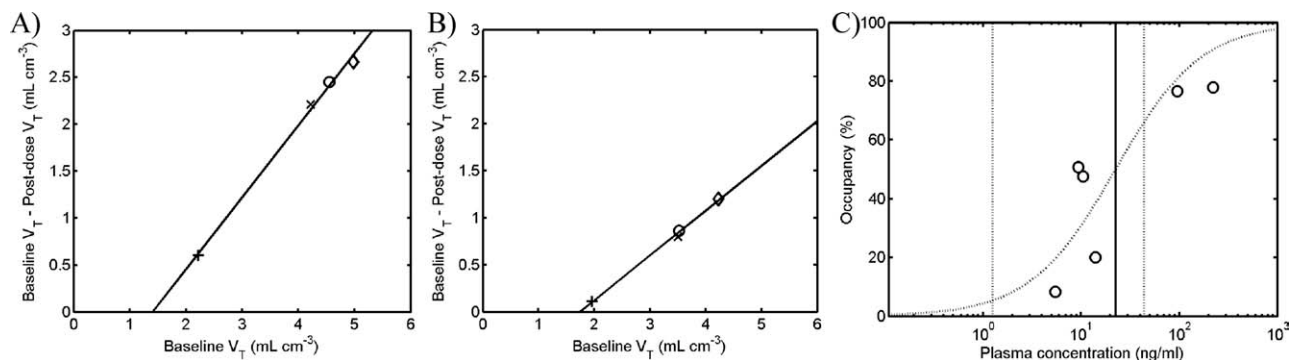


Fig. 2. [^{11}C]GSK931145 Primate data: Heterologous competition with GSK1018921. (A,B) example occupancy plot analyses for two post dose scans derived from thalamus (\diamond), cerebellum (\circ), mid brain (\times) and cortex ($+$). Slope yields occupancy and x -intercept the

V_{ND} . (C) E_{\max} model fit relating GSK1018921 plasma concentration to central GlyT-1 occupancy with the solid vertical line identifying the estimated EC_{50} and the dotted vertical lines the associated 95% confidence intervals.

across regions ($K_1 = 0.126 \pm 0.029 \text{ ml cm}^{-3} \text{ min}^{-1}$, range [0.081–0.226] across all ROIs). The distribution volume was largest in regions known to be high in GlyT-1 expression (midbrain \geq thalamus \geq cerebellum $>$ cortex) and was reduced to a homogeneous level following blocking with cold GSK931145 (0.5 mg/kg—estimated occupancy 95 and 85%). All regions in the brain displayed some level of GlyT-1 expression, and it was not possible to identify a reference tissue devoid of specific binding. Under the assumption that full block had been achieved the consequent estimates in BP_{ND} were midbrain (3.13), thalamus (2.83), cerebellum (2.53), and cortex (1.00).

In addition, a heterologous competition with GSK1018921 was performed at different doses and yielded a dose dependent reduction in V_T . Regional V_T values are given in Table I along with occupancy estimates estimated by the occupancy plot (Cunningham et al., 2010; Lassen et al., 1995; see Figs. 2A–2C). The $T_{1/2}$ of GSK1018921 in plasma was esti-

mated to be 73 min by fitting an exponential to the terminal pharmacokinetic data. A fit of the GSK1018921 occupancy data by Eq. 3 yielded an EC_{50} value of 22.5 ng/ml (95% CI: 1.3–43.7 ng/ml). This E_{\max} relationship, with E_{\max} fixed to 100%, was preferred over an alternative two parameter version with fitted E_{\max} as determined by the Akaike criterion for model selection.

Human studies

Ten out of the 17 subjects who enrolled in the test–retest study provided complete data sets (four subjects withdrew before completing more than one scan and three subjects did not provide quantifiable metabolite data from at least one scan). Ten out of the 11 subjects who enrolled in the occupancy study provided complete data sets (one subject withdrew after their baseline scan).

Following i.v. injection in humans there was distribution throughout the brain with increased uptake in

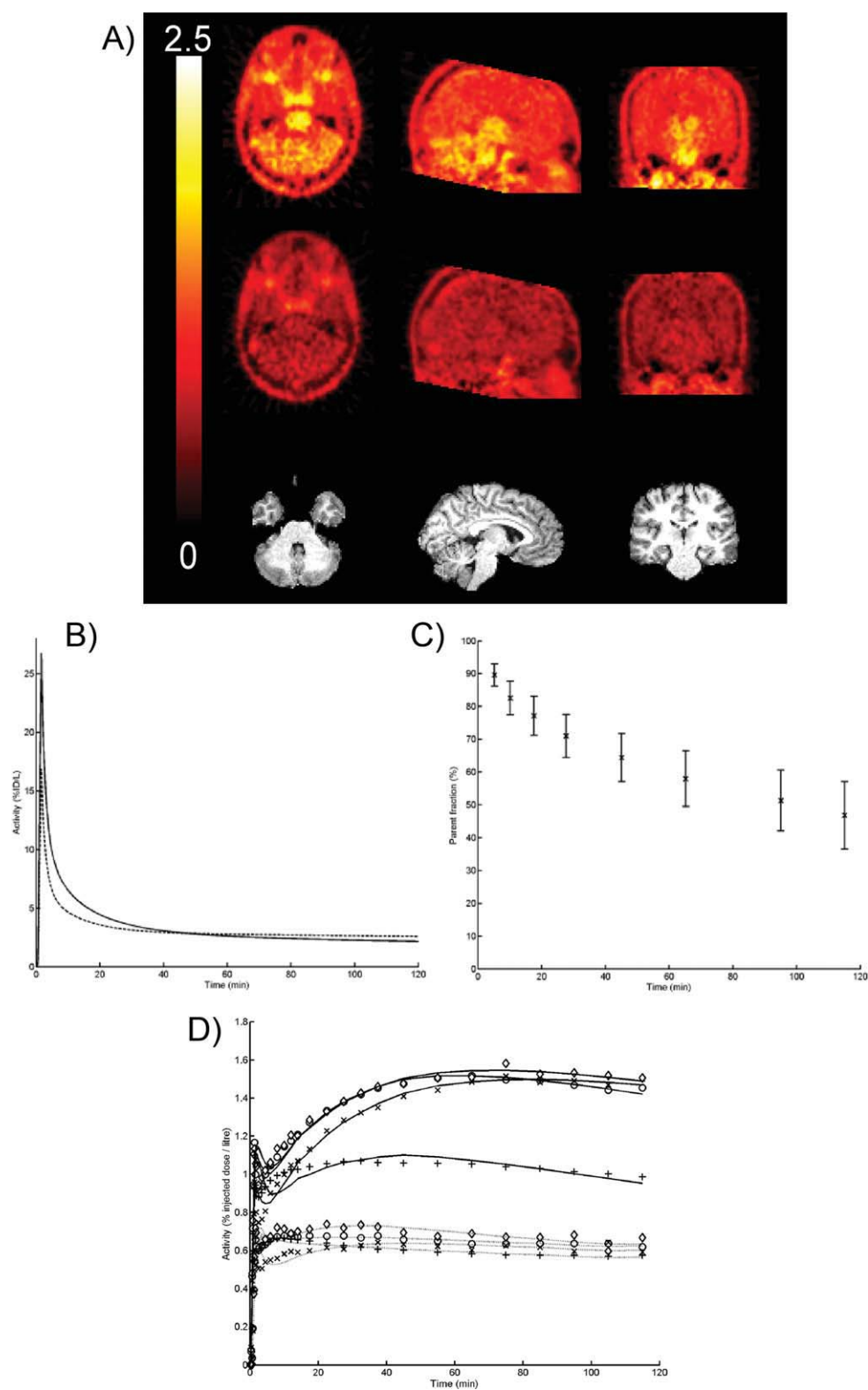


Fig. 3. $[^{11}\text{C}]\text{GSK931145}$ Human data. (A) Heterogeneous distribution in brain with high uptake in brain stem, thalamus and cerebellum at baseline (top row) homogeneous distribution following large dose (200 mg) of GSK1018921 (middle row) and structural MRI (bottom). Units are %ID/L. (B) Metabolite corrected arterial plasma time course for $[^{11}\text{C}]\text{GSK931145}$ (solid line) and

whole blood radioactivity time course (dashed line). (C) Measured $[^{11}\text{C}]\text{GSK931145}$ fraction in plasma samples. (D) Regional TACs (thalamus (\diamond), cerebellum (\circ), brain stem (\times), and cortex ($+$)) and two tissue compartment model fits from baseline scan (solid lines) following a large dose of GSK1018921 (200 mg) (dashed lines).

GlyT-1 rich areas such as cerebellum, brain stem, and thalamus similar to the primate brain (Figs. 3A and 3D). The tracer was metabolized throughout the scanning period yielding two metabolites (one polar and one lipophilic) and intact parent radioligand comprised $60 \pm 8\%$ (average over all scans) of the radioactive signal in arterial plasma after 1 h (Figs. 3B and 3C).

A 2TC model was determined as an appropriate tracer kinetic model based on the Akaike model selection criteria which preferred the reversible 2TC model over irreversible and reversible permutations of 1 and 2TC models (for brevity, only reversible 2TC results are reported). Even with the 2TC model there remained a small amount of model mismatch early on but more complex model structures were not deemed to be numerically identifiable. The 2TC model was fitted to TACs derived from cortical, cerebellar, and brain stem regions (Fig. 3D) to derive V_T estimates for all 10 test–retest scans (Table II). The V_T estimates were well identified for all five regions across all subjects as indicated by the asymptotic error estimates (mean $\%COV(V_T) = 2.31\%$). The distribution volume was largest in regions previously identified to be high in GlyT-1 expression (brain stem \geq thalamus \geq cerebellum $>$ cortex). V_T values in humans were significantly lower than those obtained in primates and this was driven by differences in K_1 (0.025 ± 0.0097 ml cm $^{-3}$ min $^{-1}$ in humans as compared to 0.126 ± 0.029 ml cm $^{-3}$ min $^{-1}$ in primates). This reduced delivery of the tracer in humans was also evident by the existence of an obvious blood volume peak at the beginning of the TACs (Fig. 2D). Time stability analysis of the V_T estimates from the 2TC model indicated that acquisitions of 60–90 min would be adequate— V_T estimates were, on average, 94% (60 min analysis) and 98% (90 min analysis) of the V_T values obtained from the full 120 min analysis when assessed across the five regions considered here.

The test–retest reproducibility of V_T calculated using the 2TC approach was poor (VAR:29–38%; ICC:0.14–0.34) for the four regions (Table II). Assessment of all regions in the CIC neuroanatomical atlas identified the middle temporal gyrus as the region with the lowest V_T value across the population of subjects. The PRTM was applied using the middle temporal gyrus as the pseudo reference tissue with an estimate of $BP_{ND}^R (= 0.56 \pm 0.30)$ derived from analysis of human GSK1018921 occupancy data (see below). This approach yielded regional BP_{ND} estimates for brain stem (1.94 ± 0.55), thalamus (1.74 ± 0.37), cerebellum (1.55 ± 0.35), and cortex (0.76 ± 0.13) for the test–retest dataset that were broadly in line with those from primate. The test–retest performance for the BP_{ND} outcome measure derived from this approach was superior to that of V_T derived from the 2TC approach with VAR ranging from 16 to 23%

TABLE II. Quantitative analysis of [^{11}C]GSK931145 human test–retest studies

Subject	Brain stem				Thalamus				Cerebellum				Cortical				Middle temporal gyrus			
	V_T		BP_{ND}		V_T		BP_{ND}		V_T		BP_{ND}		V_T		BP_{ND}		V_T		BP_{ND}	
	Scan 1	Scan 2	Scan 1	Scan 2	Scan 1	Scan 2	Scan 1	Scan 2	Scan 1	Scan 2	Scan 1	Scan 2	Scan 1	Scan 2	Scan 1	Scan 2	Scan 1	Scan 2	Scan 1	Scan 2
1f	0.42	0.46	2.48	3.23	0.38	0.33	2.15	2.02	0.35	0.31	1.87	1.84	0.23	0.20	0.88	0.79	0.19	0.17	0.56	0.56
2f	0.90	0.75	1.57	1.83	0.83	0.71	1.37	1.70	0.79	0.69	1.28	1.60	0.60	0.47	0.73	0.77	0.54	0.41	0.56	0.56
3f	1.05	1.20	2.32	2.44	0.97	1.08	2.05	2.10	0.90	1.05	1.85	2.00	0.55	0.62	0.72	0.78	0.49	0.54	0.56	0.56
4m	0.53	0.63	2.29	2.41	0.53	0.54	2.27	1.96	0.50	0.53	2.09	1.90	0.29	0.33	0.79	0.77	0.25	0.29	0.56	0.56
5f	0.63	0.54	1.92	2.33	0.55	0.50	1.54	2.12	0.51	0.45	1.40	1.79	0.36	0.33	0.67	1.06	0.33	0.25	0.56	0.56
6f	0.48	0.74	1.40	0.88	0.44	0.72	1.24	0.82	0.42	0.70	1.14	0.78	0.33	0.72	0.67	0.83	0.31	0.62	0.56	0.56
7m	1.22	0.44	1.35	1.60	1.23	0.43	1.36	1.56	1.17	0.39	1.25	1.32	0.87	0.24	0.67	0.41	0.81	0.26	0.56	0.56
8f	0.86	1.18	1.46	1.99	0.88	1.09	1.53	1.75	0.91	1.00	1.60	1.52	0.59	0.71	0.70	0.79	0.54	0.62	0.56	0.56
9f	0.94	0.73	1.87	2.34	0.91	0.66	1.79	2.03	0.82	0.60	1.51	1.75	0.56	0.38	0.72	0.74	0.51	0.34	0.56	0.56
10m	0.88	1.18	1.86	1.23	0.82	1.44	1.67	1.73	0.74	1.06	1.42	1.00	0.54	1.05	0.76	1.00	0.48	0.82	0.56	0.56
Mean \pm sd	0.79 ± 0.26	0.78 ± 0.30	1.85 ± 0.41	2.03 ± 0.68	0.75 ± 0.27	0.75 ± 0.35	1.70 ± 0.36	1.78 ± 0.39	0.71 ± 0.26	0.68 ± 0.27	1.54 ± 0.31	1.55 ± 0.40	0.49 ± 0.19	0.50 ± 0.27	0.73 ± 0.07	0.80 ± 0.17	0.45 ± 0.18	0.43 ± 0.21	0.56 ± 0.00	0.56 ± 0.00
VAR	30%	30%	23%	23%	30%	30%	16%	16%	29%	29%	16%	16%	38%	38%	18%	18%	37%	37%	0%	0%
ICC	0.36	0.36	0.67	0.67	0.34	0.34	0.68	0.68	0.36	0.36	0.73	0.73	0.14	0.14	0.05	0.05	0.21	0.21	1	1

V_T estimates were obtained from a 2TC analysis and BP_{ND} estimates were obtained from PRTM analysis. Reproducibility is quantified by VAR and ICC. m and f refer to male and female.

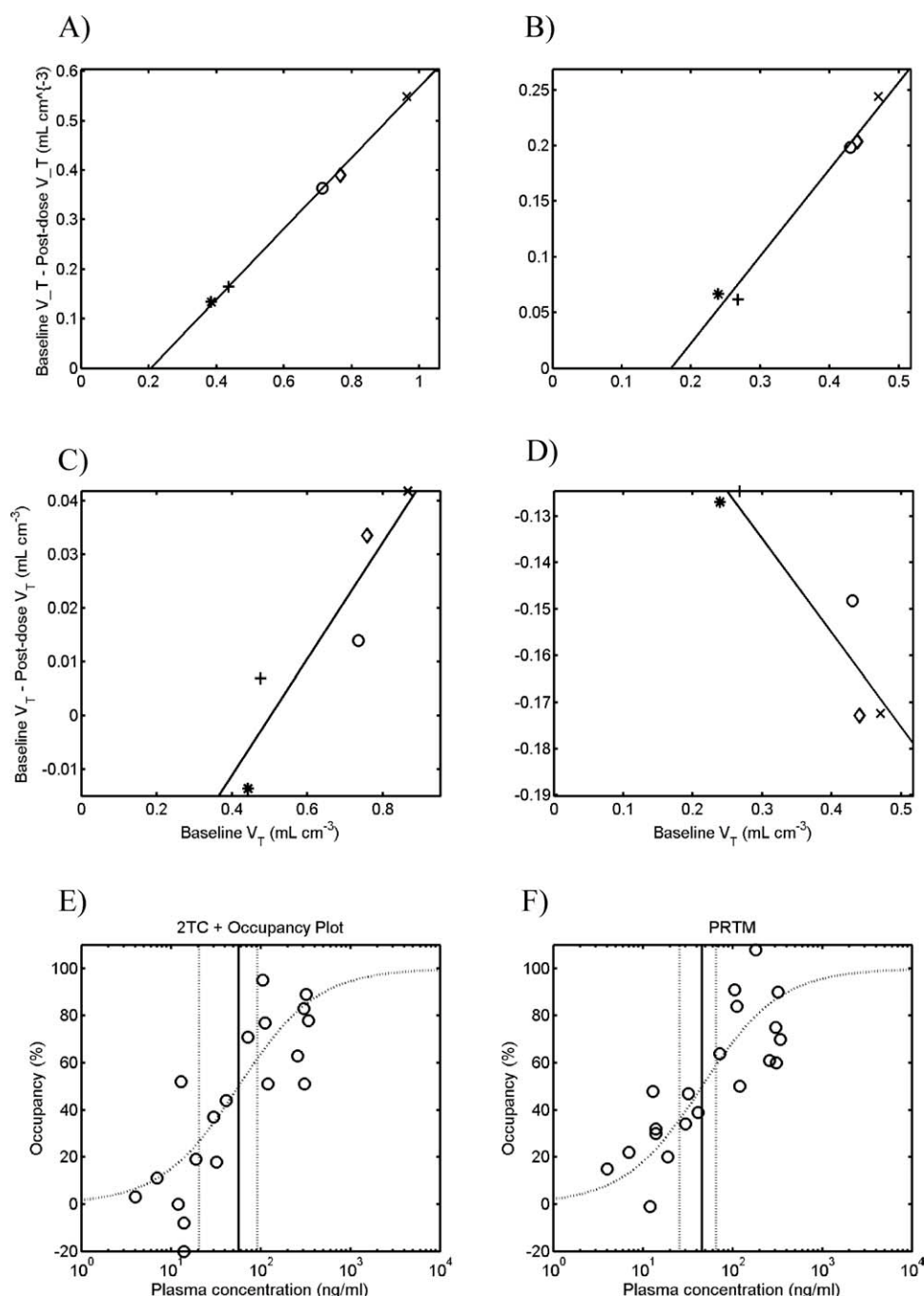


Fig. 4. GSK1018921 occupancy in humans. Example occupancy plots (A,B,C,D) derived from four post dose scans using thalamus (\diamond), cerebellum (\circ), brain stem (\times), cortex ($+$) and middle temporal gyrus ($*$). (A,B) Strong linear relationship with non-negative x -intercept and occupancy values, (C) increased noise, and (D) V_T post

dose is higher than baseline. E_{\max} model fit relating GSK1018921 plasma concentration to central GlyT-1 occupancy for occupancy results (E) derived from 2TC analysis and occupancy plot, and (F) occupancy results derived from PRTM.

instead of 29–38%. Similarly the ICC values for the GlyT-1 rich regions (brain stem, thalamus, and cerebellum) improved substantially for the pseudo reference tissue approach (ICC = 0.67, 0.68, and 0.73 when compared with 0.36, 0.34, and 0.36 for 2TC derived V_T estimates).

Data from 10 subjects, who underwent scans following oral dosing of GSK1018921, demonstrated clear evidence of occupancy at the GlyT-1 transporter with an overall reduction in standardized uptake value (SUV) and elimination of heterogeneous distribution of signal for the largest doses (Fig. 3A). In addition,



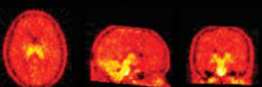
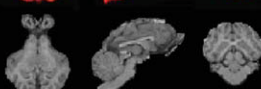
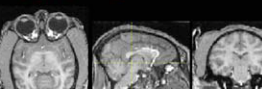

		Pig	Primate	Human
Images				
				
Cortex	f_p	0.03	0.08	0.008
	K_1	0.061	0.13	0.025
	V_T	3.87	2.39	0.49
	V_T/f_p	129	29.9	61.3

Fig. 5. $[^{11}\text{C}]\text{GSK931145}$ species differences in pig ($n = 2$), primate ($n = 8$) and human ($n = 10$). Images are representative SUV images. The parameters are plasma free fraction (f_p : unitless), tracer delivery (K_1 : $\text{mL cm}^{-3} \text{ min}^{-1}$), distribution volume (V_T : mL cm^{-3}) and distribution volume normalized to the free tracer concentration in plasma (V_T/f_p : mL cm^{-3}) in cortex.

brain stem, cerebellum, and cortex TACs collapsed on top of each other following a large dose of GSK1018921 (Fig. 3D). For large doses of GSK1018921, 2TC analyses revealed that all regions exhibited a reduction in V_T and thus no reference region was identified.

Occupancy estimates were obtained using both the occupancy plot and PRTM approach for all post dose GSK1018921 scans. Given inherent variability in the V_T values (with some post dose V_T values exceeding those at baseline), the occupancy plot did not work well for all scans (visual assessment deemed that 45% of the occupancy plots demonstrated a strong linear relationship with nonnegative x-intercept and occupancy, Figures 4A–4D). The average occupancy plot intercept from these scans was used to estimate $\text{BP}_{\text{ND}}^R = 0.56 \pm 0.30$. In contrast, occupancy values derived from PRTM showed less variance which was further evident when exploring the E_{max} relationship with the GSK1018921 plasma concentrations (Figs. 4E and 4F). The residual sum of squares (RSSQ) for the pseudo reference tissue approach was smaller ($\text{RSSQ} = 0.53$) than that obtained with occupancy plot derived estimates ($\text{RSSQ} = 1.11$). Again, the E_{max} model with E_{max} fixed to 100% (Eq. 3) was preferred over an alternative two parameter version with fitted E_{max} as determined by the Akaike criterion for model selection. The EC_{50} of GSK1018921 was estimated as 56.7 ng/ml (95% CI: 20.8–92.6 ng/ml) for the occupancy plot derived estimates and 45.7 ng/ml (95% CI: 25.6–65.8 ng/ml) for PRTM derived estimates.

DISCUSSION

$[^{11}\text{C}]\text{GSK931145}$ PET studies were successfully performed in primates and man. In primates,

$[^{11}\text{C}]\text{GSK931145}$ readily enters the brain and displays a heterogeneous uptake which corresponds well with previous pig data and the known distribution of GlyT-1 (Brain stem~Thalamus~Cerebellum>Cortex). There is a good specific signal in all regions with cortex having a BP_{ND} around 1 and the GlyT-1 rich areas having a BP_{ND} of 2 to 3. The kinetics are fast enough to allow for good estimates of V_T using a 2TC model from a 90 min scan. In humans, the tracer is metabolized more slowly and delivery of $[^{11}\text{C}]\text{GSK931145}$ to the brain is reduced with K_1 values 5-fold lower than in primate. These differences are also reflected in V_T estimates which are also about 5-fold lower in humans. However, the heterogeneous pattern of uptake is similar to that seen in primate and pig. There is a good specific signal in all regions with cortex having a BP_{ND} around 0.75 and the GlyT-1 rich areas having a BP_{ND} of around 1.5 to 2. Similarly to primates, the tracer demonstrated reversible kinetics within the time frame of the scan, and it was possible to estimate V_T from the 2TC model. In the human data sets there was some moderate model mismatch early on even with the reversible 2TC model. This should not significantly affect the estimates of the macroparameter V_T as the wash-out phase of the data is well captured by the model fit. It is not clear what drives the model mismatch in the early phase of the scan but this could be due to inaccuracies in the blood and metabolite data, errors in scanner corrections at low uptake or the presence of a brain penetrant metabolite.

Comparison of key parameters for pig, primate, and human are given in Figure 5 (pig data is taken from Passchier et al., 2010). To explore species differences further, equilibrium dialysis (Summerfield et al., 2006) estimates of the free fraction of tracer in

plasma (f_P) were obtained. The f_P in humans (0.8%) was lower than in pig (3%) and primate (8%) and would consequently drive similar reductions in K_1 and V_T . When V_T is normalized by f_P to give the partition coefficient with free plasma the measures are more in agreement across species (Fig. 5).

Test-retest performance of [^{11}C]GSK931145 in humans with the 2TC analysis was poor ($\text{VAR}(V_T)$:29–38%). A simple examination of test-retest variability of the individual total plasma SUV, metabolite fraction, and brain SUV measurements (mean value between 60 and 90 min) indicated that variability in V_T estimates was likely partitioned equally among the three measurements supporting the advantage of a reference region approach. The application of PRTM improved the test-retest performance of [^{11}C]GSK931145 ($\text{VAR}(\text{BP}_{\text{ND}})$:16–23%). This improvement in reproducibility for reference region based outcome measures is evident for other radioligands (see Table III; $\text{VAR}(\text{BP}_{\text{ND}}) = 0.71 (\pm 0.076) \text{VAR}(V_T)$). Application of PRTM can be extended by employing SRTM (Gunn et al., 1997; Lammertsma and Hume, 1996) instead of a 2TC analysis which obviates the need for blood sampling. We explored the relationship between the outcome measures derived for both the 2TC and SRTM based PRTM approaches and were able to show that they were in good agreement (data not shown). However, even with the PRTM approach, performance of [^{11}C]GSK931145 is at best moderate.

To further investigate the human reproducibility data and species differences, we examined data from a number of established PET radioligands (Table III). While for all radioligands there was a tendency for the plasma free fraction to be smaller in humans (apart from [^{11}C]NPA), the order of magnitude reduction observed for [^{11}C]GSK931145 was unusually large. The K_1 was lower in humans for all radioligands and so was the V_{ND} (apart from [^{11}C]NPA). Calculation of the free partition coefficient (V_{ND}/f_P) removed this evident decrease across species. The tendency for plasma clearance (CL) was for it to increase in humans although raclopride decreased and [^{11}C]GSK931145 remained unchanged. Thus, the 10-fold reduction in plasma free fraction for [^{11}C]GSK931145 and the low K_1 in humans stand out among these data.

A reduction in K_1 and associated loss of signal-to-noise in brain TACs would be expected to reduce the performance of a radioligand, and this has been captured recently by the biomathematics of Guo et al. (2009). Examination of parameters for different radioligands indicates that the K_1 for [^{11}C]GSK931145 is by far the lowest. Comparison of [^{11}C]GSK931145 performance ($\text{VAR}(V_T)$:32%, $\text{VAR}(\text{BP}_{\text{ND}})$:18%) with the best performing radioligand, [^{11}C]raclopride ($\text{VAR}(V_T)$:5%, $\text{VAR}(\text{BP}_{\text{ND}})$:4%), is noteworthy, with similar values for V_{ND} (0.3, 0.4 ml cm^{-3}), BP_{ND} (2, 3), and CL (8, 14 L hr^{-1}) but 5-fold lower values for f_P

TABLE III. PET radioligands comparison of species differences and human reproducibility data

Radioligand	Target	Species	Parameters					Test retest studies				References
			f_P (%)	K_1 (mL $\text{cm}^{-3} \text{min}^{-1}$)	V_{ND} (mL cm^{-3})	$V_{\text{ND}}/f_P \cdot 3$ (mL cm^{-3})	CL (L hr^{-1})	Interval	V_T	BP_{ND}	VAR	
[^{11}C]GSK931145	GlyT-1	Human	0.8%	0.03	0.31	39	8	> 6 days	32	18		Parsey et al, 2000
[^{11}C]WAY100635	5HT $_{1A}$	Primate	8.0%	0.13	1.64	21	9	same day	21	16		Slifstein (pers. comm.)
		Human	5.8%	0.08	0.89	15	180					Abi Dargham et al, 2000
[^{11}C]NINC112	D1	Primate	15.0%	0.25	1.08	7	23	same day	8	6		Slifstein et al, 2011
		Human	1.0%	0.13	2.10	210	96					Narendran et al, 2011
[^{11}C]NPA	D2	Primate	2.0%	1.07	5.15	258	59	same day	8	5		Hwang et al, 2004
		Human	11.0%	0.27	4.03	37	119					Frankle et al, 2006
[^{11}C]DASB	SERT	Primate	4.9%	0.91	3.44	70	29	same day	7	5		Huang et al, 2002
		Human	9.4%	0.54	9.50	101	163					Mawlawi et al, 2001
[^{11}C]Raclopride	D2	Primate	13.5%	1.36	17.30	128	84	same day	5	4		Slifstein et al, 2011
		Human	3.5%	0.13	0.42	12	14					
		Primate	13.0%	0.28	0.97	7	33					

f_P is plasma free fraction, K_1 is brain delivery, V_{ND} is the nondisplaceable distribution volume, CL is the plasma clearance and is calculated as the ratio of the injected dose to the area under the curve of the input function (Rowland and Tozer, 1989). V_T results are derived from 2TC analyses apart from [^{11}C] raclopride which is derived from a tissue to plasma ratio at equilibrium. BP_{ND} results are obtained from reference tissue based methods.

(0.8,3.5%) and K_1 (0.025,0.13 ml cm⁻³ min⁻¹). However, a 5-fold reduction in K_1 on its own would not be expected to result in the poor reproducibility data observed with [¹¹C]GSK931145, with signal-to-noise expected to drop at best in line with the square root of activity (i.e., $\sqrt{5} = 2.2$).

Thus, it is unlikely that the low delivery is the only reason for the poor reproducibility of [¹¹C]GSK931145. It is of interest to note that the other test-retest studies with lower variability involved subjects scanned on the same day (Table III). Here, the scans were performed at least 6 days apart and additional variability in the biological measurements over this time period could be a contributory factor. Further studies would be required to test this hypothesis with test-retest data obtained on the same and different days in all subjects. If this difference is real, then it would be important to plan test-retest data acquisition to match subsequent experimental designs.

Even though performance of [¹¹C]GSK931145 was modest, the tracer was successfully used in drug development studies of GSK1018921 in primates and humans to measure occupancy of the novel GlyT-1 inhibitor. GSK1018921 demonstrated clear blood brain barrier penetration in primates and humans with similar EC₅₀ values of 22.5 and 45.7 ng/ml, respectively, (overlapping 95% CI) that become even closer when accounting for the GSK1018921 plasma free fraction (16% in primate and 6% in humans). In humans, PRTM again demonstrated superior quantification over the 2TC based method, although 2TC results were acceptable.

Therefore, while GlyT-1 imaging with [¹¹C]GSK931145 is acceptable for occupancy studies, it is unlikely that this will be a good enough tool to explore differences in target expression and function in different clinical populations. In such studies, it is necessary to account for nonspecific binding differences between populations, which means using a plasma based outcome measure and f_P (which may not be measurable here). This would also likely require an additional scan with a GlyT-1 inhibitor in order to calculate the tissue nonspecific binding in each subject/population.

A novel PET imaging probe for GlyT-1 and its translation into primate and man has been presented. [¹¹C]GSK931145 has immediate importance in the assessment of novel GlyT-1 inhibitors as medicines for diseases such as schizophrenia. Such imaging tools can provide critical information for drug development teams to reduce risk, advance effective molecules, and efficiently design later phase efficacy trials.

ACKNOWLEDGMENTS

The authors thank Jan Passchier for implementing radiochemistry; Natalia Lopez-Vilanova for acquiring

PET and blood data in the human studies; Joaquim Radua for drafting the human subjects section; John Castrillon and Balu Easwaramoorthy for radiochemistry production at Columbia University; Elizabeth Hackett, Sung A Bae, and Xiaoyan Xu for data acquisition and data management at Columbia University; the staff at Pharmacology Unit, IMIM, Barcelona for recruitment and care of volunteers; and the staff at Molecular Imaging Center, Barcelona for performing the PET scans.

REFERENCES

- Abi-Dargham A, Martinez D, Mawlawi O, Simpson N, Hwang DR, Slifstein M, Anjilvel S, Pidcock J, Guo NN, Lombarde I, Mann JJ, Van Heertum R, Fotedar C, Halldin C, Laruelle M. 2000. Measurement of striatal and extrastriatal dopamine D1 receptor binding potential with [¹¹C]NNC 112 in humans: Validation and reproducibility. *J Cereb Blood Flow Metab* 20:225–243.
- Aragon C, Lopez-Corcuera B. 2005. Glycine transporters: Crucial roles of pharmacological interest revealed by gene deletion. *Trends Pharmacol Sci* 26:283–286.
- Asselin M-C, Montgomery AJ, Grasby PM, Hume SP. 2007. Quantification of PET studies with the very high affinity dopamine D2/D3 receptor ligand [¹¹C]FLB457: Re-evaluation of the validity of using a cerebellar reference region. *J Cereb Blood Flow Metab* 27:378–392.
- Brix G, Zaers J, Adam L-E, Bellemann ME, Ostertag H, Trojan H, Haberkorn U, Doll J, Oberdorfer F, Lorenz WJ. 1997. Performance evaluation of a whole-body PET scanner using the NEMA protocol. *J Nucl Med* 30:1614–1623.
- Bullich S, Slifstein M, Passchier J, Murthy NV, Kegeles LS, Kim JH, Xu X, Gunn RN, Herance R, Gispert JD, Gutiérrez A, Farré M, Laruelle M, Catafau AM. 2010. Biodistribution and radiation dosimetry of the glycine T1 transporter ligand [¹¹C]-GSK931145 determined from primate and human whole-body PET. *Mol Imaging Biol*. Doi: 10.1007/s11307-010-0398-6.
- Christian BT, Narayanan T, Shi B, Morris ED, Mantil J, Mukherjee J. 2004. Measuring the in vivo binding parameters of [¹⁸F]-flupyridine in monkeys using a PET multiple-injection protocol. *J Cereb Blood Flow Metab* 24:309–322.
- Cubelos B, Gimenez C, Zafra F. 2005. Localization of the GLYT-1 glycine transporter at glutamatergic synapses in the rat brain. *Cereb Cortex* 15:448–459.
- Cunningham VJ, Rabiner EA, Slifstein M, Laruelle M, Gunn RN. 2010. Measuring drug occupancy in the absence of a reference region: The Lassen plot re-visited. *J Cereb Blood Flow Metab* 30:46–50.
- First MB, Spitzer RL, Gibbon M, Williams JBW. 2002. Structured clinical interview for DSM-IV-TR axis I disorders (SCID-I). New York: Biometrics Research, New York State Psychiatric Institute.
- Frankle WG, Slifstein M, Gunn RN, Huang Y, Hwang DR, Darr EA, Narendran R, Abi-Dargham A, Laruelle M. 2006. Estimation of serotonin transporter parameters with [¹¹C]-DASB in healthy humans: Reproducibility and comparison of methods. *J Nucl Med* 47:815–826.
- Gunn RN, Lammertsma AA, Hume SP, Cunningham VJ. 1997. Parametric imaging of ligand-receptor binding in PET using a simplified reference tissue model. *NeuroImage* 6:279–287.
- Guo Q, Brady M, Gunn RN. 2009. A biomathematical modeling approach to central nervous system radioligand discovery and development. *J Nucl Med* 50:1715–1723.
- Hamill TG, Eng W, Jennings A, Lewis R, Thomas S, Wood S, Street L, Wisnoski D, Wolkenberg S, Lindsley C, Sanabria-Bohorquez S, Patel S, Riffel K, Ryan C, Cook J, Sur C, Burns D, Hargreaves R. 2011. The synthesis and preclinical evaluation in Rhesus monkey of [¹⁸F]MK-6577 and [¹¹C]CMPyPB, glycine transporter 1 (GlyT1) PET radiotracers. *Synapse* 65:261–270.
- Huang Y, Hwang DR, Narendran R, Sudo Y, Chatterjee R, Bae SA, Mawlawi O, Kegeles LS, Wilson AA, Kung HF, Laruelle M. 2002. Comparative evaluation in nonhuman primates of five PET radiotracers for imaging the serotonin transporters: [¹¹C]MeN 5652, [¹¹C]ADAM, [¹¹C]DASB, [¹¹C]DAPA, and [¹¹C]AFM. *J Cereb Blood Flow Metab* 22:1377–1398.

- Hwang DR, Narendran R, Huang Y, Slifstein M, Talbot PS, Sudo Y, Van Berckel BN, Kegeles LS, Martinez D, Laruelle M. 2004. Quantitative analysis of (-)-N-(11)C-propyl-norapomorphine in vivo binding in nonhuman primates. *J Nucl Med* 45:338–346.
- Kirk RE. 1982. Experimental design: Procedures for the behavioral sciences. Pacific Grove, CA: Brooks/Cole Publishing.
- Lammertsma AA, Hume SP. 1996. Simplified reference tissue model for PET receptor studies *NeuroImage* 4:153–158.
- Lane HY, Chang YC, Liu YC, Chiu CC, Tsai G. 2005. Sarcosine or D-serine add-on treatment for acute exacerbation of schizophrenia. *Arch Gen Psychiatry* 62:1196–1204.
- Lassen NA, Bartenstein PA, Lammertsma AA, Prevett MC, Turton DR, Luthra SK, Osman S, Bloomfield PM, Jones T, Patsalos PN, O'Connell MT, Duncan JS, Andersen JV. 1995. Benzodiazepine receptor quantification in vivo in humans using [11C]flumazenil and PET: Application of the steady-state principle. *J Cereb Blood Flow Metab* 15:152–165.
- Mawlawi O, Martinez D, Slifstein M, Broft A, Chatterjee R, Hwang DR, Huang Y, Simpson N, Ngo K, Van Heertum R, Laruelle M. 2001. Imaging human mesolimbic dopamine transmission with positron emission tomography. I. Accuracy and precision of D(2) receptor parameter measurements in ventral striatum. *J Cereb Blood Flow Metab* 21:1034–1057.
- Narendran R, Frankle W, Mason NS, Laymon CM, Lopresti BJ, Price JC, Kendro S, Vora S, Litschge M, Mountz JM, Mathis CA. 2009. Positron emission tomography imaging of D(2/3) agonist binding in healthy human subjects with the radiotracer [(11)C]-N-propyl-norapomorphine: Preliminary evaluation and reproducibility studies. *Synapse* 63:574–584.
- Olsson H, Halldin C, Farde L. 2004. Differentiation of extrastriatal dopamine D2 receptor density and affinity in the human brain using PET. *NeuroImage* 22:794–803.
- Parsey RV, Slifstein M, Hwang DR, Abi-Dargham A, Simpson N, Mawlawi O, Guo NN, Van Heertum R, John Mann J, Laruelle M. 2000. Validation and reproducibility of measurement of 5-HT1A receptor parameters with [carbonyl-11C]WAY-100635 in humans: Comparison of arterial and reference tissue input functions. *J Cereb Blood Flow Metab* 20:1111–1133.
- Passchier J, Gentile G, Porter R, Herdon H, Salinas C, Jakobsen S, Audrain H, Laruelle M, Gunn RN. 2010. Identification and evaluation of [11C]GSK931145 as a novel ligand for imaging the type 1 glycine transporter with positron emission tomography. *Synapse* 64:542–549.
- Rowland M, Tozer TN. 1989. Clinical pharmacokinetics, 2nd ed. Philadelphia: Lea & Febiger.
- Slifstein M, Suckow RF, Javitch JA, Cooper T, Lieberman J, Abi-Dargham A. 2011. Characterization of in vivo pharmacokinetic properties of the dopamine D1 receptor agonist DAR-0100A in nonhuman primates using PET with [(11)C]NINC112 and [(11)C]raclopride. *J Cereb Blood Flow Metab* 31:293–304.
- Summerfield SG, Stevens AJ, Cutler L, Osuna MDC, Hammond B, Tang SP, Hersey A, Spalding DJ, Jeffrey P. 2006. Improving the in vitro prediction of in vivo central nervous system penetration: Integrating permeability, P-glycoprotein efflux, and free fractions in blood and brain. *J Pharmacol Exp Ther* 316:1282–1290.
- Tsai G, Lane HY, Yang P, Chong MY, Lange N. 2004. Glycine transporter 1 inhibitor N-methylglycine (sarcosine). Added to antipsychotics for the treatment of schizophrenia. *Biol Psychiatry* 55:452–456.
- Tziortzi AC, Searle GE, Tzimopoulou S, Salinas C, Beaver JD, Jenkinson M, Laruelle M, Rabiner EA, Gunn RN. 2010. Imaging dopamine receptors in humans with [11C]-(+)-PHNO: Dissection of D3 signal and anatomy. *NeuroImage* 54:264–277.
- Watson CC. 1996. Technique for measuring the energy response of a PET tomograph using a compact scattering source. *IEEE Nuclear Science Symposium and Medical Imaging Conference*. p1562–1566.
- Zamuner S, Di Iorio VL, Nyberg J, Gunn RN, Cunningham VJ, Gomeni R, Hooker AC. 2010. Adaptive-optimal design in PET occupancy studies. *Clin Pharmacol Ther* 87:563–571.

APPENDIX: DERIVATION OF PSEUDO REFERENCE TISSUE MODEL (PRTM) EQUATIONS

Derivation of Eq. 1. Let BP_{ND}^M denote the binding potential measured for T by treating the pseudo reference region R as a true reference region:

$$BP_{ND}^M = \frac{V_T^T - V_T^R}{V_T^R} \quad (A1)$$

Dividing top and bottom by V_{ND} gives

$$BP_{ND}^M = \frac{BP_{ND}^T - BP_{ND}^R}{1 + BP_{ND}^R} \quad (A2)$$

and then rearranging yields the general correction,

$$BP_{ND}^T = BP_{ND}^R + BP_{ND}^M (1 + BP_{ND}^R). \quad (A3)$$

Derivation of Eq. 2. Consider a PET experiment consisting of two PET scans (baseline followed by postdrug), and resulting data for a target region T and a pseudo reference region R of low but nonzero binding. Let V_T^{T1} and V_T^{T2} be the total volume of distribution measured in the target region in scans 1 and 2, respectively, and let V_T^{R1} and V_T^{R2} be the corresponding volumes of distribution in the pseudo reference region.

Measured binding potentials for T can be calculated for scans 1 and 2 in the standard way (i.e., as though R were a true reference region) from the volumes of distribution:

$$\begin{aligned} BP_{ND}^{M1} &= \frac{V_T^{T1} - V_T^{R1}}{V_T^{R1}} \\ BP_{ND}^{M2} &= \frac{V_T^{T2} - V_T^{R2}}{V_T^{R2}}. \end{aligned} \quad (A4)$$

Occupancy by the drug can also be calculated in the standard way, giving an uncorrected measured occupancy:

$$Occ^M = \frac{BP_{ND}^{M1} - BP_{ND}^{M2}}{BP_{ND}^{M1}}. \quad (A5)$$

Substituting A4 into A5 and using $V_T = V_{ND} + V_S$ gives:

$$\text{Occ}^M = \frac{\frac{V_T^{T1} - V_T^{R1}}{V_T^{R1}} - \frac{V_T^{T2} - V_T^{R2}}{V_T^{R2}}}{\frac{V_T^{T1} - V_T^{R1}}{V_T^{R1}}} \quad \text{Occ}^M = \frac{V_{\text{ND}} - \frac{V_S^{T2}}{V_S^{T1}} V_{\text{ND}}}{(V_S^{R2} + V_{\text{ND}})}. \quad (\text{A9})$$

$$\begin{aligned} &= 1 - \frac{V_T^{R1}}{V_T^{R2}} \left(\frac{V_T^{T2} - V_T^{R2}}{V_T^{T1} - V_T^{R1}} \right) \quad (\text{A6}) \quad \text{Rearranging yields} \\ &= 1 - \frac{V_T^{R1}}{V_T^{R2}} \left(\frac{V_S^{T2} - V_S^{R2}}{V_S^{T1} - V_S^{R1}} \right). \end{aligned}$$

Now, if we assume that fractional occupancy is the same in T and R (i.e., $\frac{V_S^{T2}}{V_S^{T1}} = \frac{V_S^{R2}}{V_S^{R1}}$) then,

$$\begin{aligned} \text{Occ}^M &= 1 - \frac{V_T^{R1}}{V_T^{R2}} \left(\frac{V_S^{T2} - V_S^{R1} \frac{V_S^{T2}}{V_S^{T1}}}{V_S^{T1} - V_S^{R1}} \right) \\ &= 1 - \frac{V_T^{R1}}{V_T^{R2}} \left(\frac{V_S^{T2}}{V_S^{T1} - V_S^{R1}} \right) \left(1 - \frac{V_S^{R1}}{V_S^{T1}} \right) \quad (\text{A7}) \\ &= 1 - \frac{V_T^{R1}}{V_T^{R2}} \frac{V_S^{T2}}{V_S^{T1}}. \end{aligned}$$

Again using $V_T = V_{\text{ND}} + V_S$, V yields

$$\begin{aligned} \text{Occ}^M &= 1 - \left(\frac{V_S^{R1} + V_{\text{ND}}}{V_S^{R2} + V_{\text{ND}}} \right) \frac{V_S^{T2}}{V_S^{T1}} \\ &= \frac{V_S^{T1} V_S^{R2} + V_S^{T1} V_{\text{ND}} - V_S^{T2} V_S^{R1} - V_S^{T2} V_{\text{ND}}}{V_S^{T1} (V_S^{R2} + V_{\text{ND}})} \\ &= \frac{V_S^{R2} + V_{\text{ND}} - \frac{V_S^{T2}}{V_S^{T1}} V_S^{R1} - \frac{V_S^{T2}}{V_S^{T1}} V_{\text{ND}}}{(V_S^{R2} + V_{\text{ND}})} \quad (\text{A8}) \end{aligned}$$

and again since we assume homogenous occupancy ($[V_S^{T2}/V_S^{T1}] = [V_S^{R2}/V_S^{R1}]$):

$$\begin{aligned} \text{Occ}^M &= \frac{V_{\text{ND}}}{(V_S^{R2} + V_{\text{ND}})} \left(1 - \frac{V_S^{T2}}{V_S^{T1}} \right) \\ &= \frac{V_{\text{ND}}}{\left(\frac{V_S^{T2}}{V_S^{T1}} V_S^{R1} + V_{\text{ND}} \right)} \left(1 - \frac{V_S^{T2}}{V_S^{T1}} \right). \quad (\text{A10}) \end{aligned}$$

Now, since the true fractional occupancy is given by $\text{Occ} = 1 - \frac{V_S^{T2}}{V_S^{T1}}$,

$$\begin{aligned} \text{Occ}^M &= \frac{V_{\text{ND}}}{(1 - \text{Occ}) V_S^{R1} + V_{\text{ND}}} \text{Occ} \\ &= \frac{1}{(1 - \text{Occ}) \frac{V_S^{R1}}{V_{\text{ND}}} + 1} \text{Occ}. \quad (\text{A11}) \end{aligned}$$

Substituting baseline binding potential in the pseudoreference region, $\text{BP}_{\text{ND}}^{R1} = \frac{V_S^{R1}}{V_{\text{ND}}}$, gives:

$$\text{Occ}^M = \frac{1}{(1 - \text{Occ}) \text{BP}_{\text{ND}}^{R1} + 1} \text{Occ}. \quad (\text{A12})$$

Rearranging gives a correction which can be applied to measured occupancy values to recover true occupancies, given knowledge of the baseline BP in the pseudo reference region:

$$\text{Occ} = \text{Occ}^M \cdot \frac{(1 + \text{BP}_{\text{ND}}^{R1})}{(1 + \text{BP}_{\text{ND}}^{R1} \text{Occ}^M)}. \quad (\text{A13})$$